Quantum noninvasive three-component beam-spin polarimetry in the Hadron Storage Ring of the Electron-Ion Collider

Frank Rathmann

Brookhaven National Laboratory, Upton, New York

July 1, 2026

Based on https://arxiv.org/abs/2606.22265

Outline

Why non-invasive polarimetry?

Today: scattering-based polarimetry [1]

- **pC**: elastic proton-carbon scattering off a thin carbon strip, fast *relative* measurement
- **HJET**: CNI scattering off a polarized H jet, *absolute* calibration
- Invasive: beam losses, target heating; carbon strips have finite lifetime margins (previous talk)

What scattering cannot provide

- full vector (P_x, P_y, P_z): bunch by bunch, continuous
- spin tune ν_s as a precision machine diagnostic [2, 3, 4]

EIC HSR raises the bar

	RHIC pp	EIC HSR
Bunch spacing (ns)	106.6	11.0
Bunches per ring	111	1160
N_p per bunch (10^{11})	2.0	0.69
Average current (A)	~ 0.3	~ 1.0

EIC flattop values: Tab. II of Ref. [1]; RHIC: typical polarized-proton stores.

> *Scattering reaches its EIC limits; a non-invasive pickup opens $\vec{P}$ and ν_s as new observables.*

EIC polarimetry requirements

The EIC physics program requires $\delta P/P \leq 1\%$ on the full polarization vector $\vec{P} = (P_x, P_y, P_z)$, bunch by bunch and continuously through the fill [5].

Method	(P_x, P_y)	P_z	bunch by bunch	continuous $\vec{P}(t)$
pC, relative [1]	✓	×	✓	×
HJET, absolute [6]	✓	(✓)	×	(✓)
pC/STAR + spin rotations [7]	(✓)	(✓)	×	×
SQUID pickup (this talk)	✓	✓	✓	✓

(✓): dedicated, time-averaged procedures only. HJET P_z (target reorientation) needs spin-correlation parameters not yet measured, and even then follows $\vec{P}(t)$ only ∼hourly, never bunch-resolved. pC has no P_z (parity-forbidden).

> *No scattering method gives the full vector bunch by bunch and continuously; 3D at all still awaits unmeasured inputs.*

The idea: read the magnetic moment of the bunch ▸ parameters

- A polarized bunch carries a **macroscopic magnetic dipole moment** from its aligned proton spins
- A SQUID pickup senses this field directly: **no target, no scattering, no beam loss**
- Two modes:
  - **static** (continuous, no spin manipulation), and
  - **dynamic** (FID after a small tipping pulse)

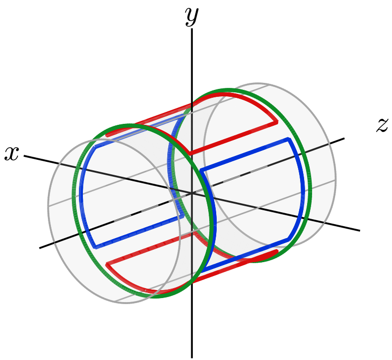

Three-channel pickup basis on a common cylindrical support. SQUID detection at RHIC proposed in [8].

> *The full vector (P_x, P_y, P_z) at a single station, continuous and bunch by bunch.*

Six Siberian snakes fix $\nu_s = 1/2$ ‣ spin matrices

- Six helical snakes, one per straight section; each rotates the spin by 180° about a horizontal axis
- Arranged as three pairs with perpendicular axes: the one-turn spin tune is $\nu_s = \frac{1}{2}$ **independent of** $G\gamma$ [9]
- Lee-Courant axis pattern $\phi_k = (-1)^{k+1} \times 45°$: stable spin axis in the arcs $\vec{n}_0 \simeq \vec{e}_y$
- When snake currents actively ramped to hold $\nu_s = 0.5$ at all energies, no first-order imperfection or intrinsic resonance crossing

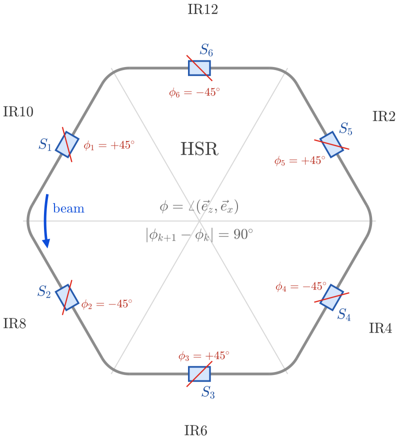

Hexagonal representation of the HSR: six arcs, six snakes $S_1, \ldots, S_6$ at IR2–IR12; red lines mark LC rotation axes.

The snake configuration fixes $\nu_s = 1/2$ at every energy and keeps $\vec{n}_0$ vertical in the arcs.

Spin precession at $\nu_s = 1/2$: signal at $f_{\rm rev}/2$ phasor

- A spin component $\perp \vec{n}_0$ advances by π per turn: the transverse magnetic moment m_x **reverses sign every turn**

$$f_s = \nu_s\, f_{\rm rev} \simeq \tfrac{1}{2} f_{\rm rev} \approx 39\,\text{kHz}$$

- Charge-current field stays on the revolution harmonics: spin and charge signals are **separated in frequency**
- 39 kHz lies in the white-noise band of wideband DC SQUID readout

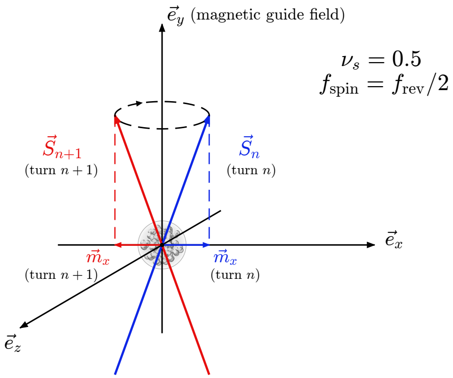

Tipping pulse creates transverse moment $\vec{m}$; for $\nu_s = 0.5$ the $\vec{e}_x$ projection flips between turns n and $n+1$.

The spin lattice moves the tiny spin signal away from the huge charge-current background.

Where $\nu_s = 1/2$ and $\vec{n}_0 \simeq \vec{e}_y$ come from

One-turn spin map

- Thomas-BMT sets precession [10]: in a vertical arc field the spin turns by $G\gamma\,\theta$ about $\vec{e}_y$
- One turn is the ordered product of arc rotations $\mathrm{R}_y(G\gamma\theta)$ and the six 180° snake flips [11]: $\mathrm{M} \in SO(3)$
- Eigenvalues $\{+1, e^{\pm 2\pi i \nu_s}\}$: the $\lambda = +1$ eigenvector is the stable axis $\vec{n}_0$

$$\boxed{\mathrm{tr}\,\mathrm{M} = 1 + 2\cos(2\pi\nu_s)}$$

Two robust consequences

- Every snake sends $S_y \to -S_y$; six of them restore it, so $\vec{n}_0 = \vec{e}_y$ in the arcs, independent of energy
- In the xz plane the per-arc phase $G\gamma\,\pi/3$ cancels pairwise across each arc-snake pair: the one-turn phase depends only on the snake-axis differences, not on $G\gamma$
- Lee-Courant axes $\phi_k = (-1)^{k+1}\,45^\circ$ give total phase π, hence $\mathrm{tr}\,\mathrm{M} = -1$ and $\nu_s = 1/2$ [9]

Full T-BMT reduction, arc and snake matrices, and the phasor cancellation: backup.

> *$\nu_s = 1/2$ and $\vec{n}_0 \simeq \vec{e}_y$ are eigenstructure of the one-turn map, not tuned conditions: robust at every energy.*

The stable spin axis $\vec{n}_0(s)$ around the ring ▸ snake axes

- Gray curve: the closed orbit; black squares: the six snakes $S_1, \dots, S_6$
- **Red**: the stable axis $\vec{n}_0(s)$ transported turn by turn, reoriented only at the snakes, vertical ($\simeq \vec{e}_y$) through the arcs
- **Blue**: spin vectors on the local precession cone; their spread is phase around $\vec{n}_0$, not successive turns

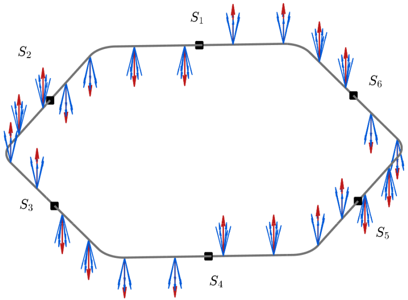

Numerical six-snake LC model. Opening angle $\psi = 30^\circ$ shown for illustration; the physical FID tip is much smaller, $\alpha = 30\,\mathrm{mrad}$.

$\vec{n}_0$ rides vertical through all arcs and tips only at snakes; spins precess about it.

Three-channel pickup basis ▸ coil geometry

Three channels, one former

- $r_{\text{coil}} = 40\,\text{mm}$
- cosine-θ saddle $\to P_x$
- sine-θ saddle, rotated 90°, $\to P_y$
- axial coaxial-loop gradiometer $\to P_z$

Charge field rejected three ways

- saddles: the first-harmonic winding cancels the symmetric current field (no $m = 1$ term for a centered beam)
- axial loop: blind by geometry; the gradiometer also cancels uniform B_z

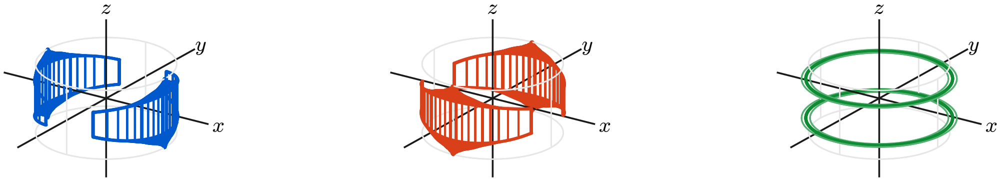

Pickup-coil geometries on common former:cos θ (P_x), sin θ (P_y), axial gradiometer (P_z); turns reduced to 10 for clarity.

Arcs: $\vec{n}_0 \simeq \vec{e}_y$, transverse channels lead, axial completes the basis; charge field rejected channel by channel.

Two operating modes: static and dynamic

Static: continuous vector

- No spin manipulation: read the bunch moment $\vec{m} = N_p \mu_p \vec{P}$ as each bunch passes
- Vertical P_y: steady on the precession scale, pulses at $f_{\rm rev}$
- Residual P_x, P_z: oscillate at $f_s = f_{\rm rev}/2$, alternating bunch to bunch
- Beam-synchronous matched filter: quasi-continuous $\vec{P}(t)$, bunch resolved

Dynamic: FID for precision on $|\vec{P}|$

- A small tip $\alpha = 30\,$mrad sets a transverse moment precessing at $f_s \approx 39\,$kHz
- Stage 1, spectral search: one short record, SNR of order unity, fixes f_s and the spread σ_{ν_s}
- Stage 2, coherent integration: many tip, read, restore cycles summed; restore loss $\mathcal{O}(\alpha^2/\pi^2) \sim 10^{-4}$ per cycle
- Precision on $|\vec{P}|$ improves as $T^{-1/2}$, polarization preserved

Dynamic-mode precession phase tracked by a reference oscillator phase-locked to f_s [12].

Static delivers the continuous vector; dynamic delivers the precision magnitude. One pickup, two complementary modes.

Net magnetic moment of a polarized bunch

Proton moment

- $\mu_p = (1+G)\mu_N = 1.4106 \times 10^{-26}\,\mathrm{J\,T^{-1}}$,
- $G = 1.7928$ [13].

$$\boxed{\vec{m} = P\, N_p\, \mu_p\, \vec{e}_y}$$

- Scale: $|m|^{\text{inj}} \approx 3.89 \times 10^{-15}\,\mathrm{J\,T^{-1}}$, $|m|^{\text{flat}} \approx 9.73 \times 10^{-16}\,\mathrm{J\,T^{-1}}$ (fourfold drop from RF splitting)
- Once tipped, $\nu_s = 1/2$ flips it each turn, $m_x(n) = PN_p\mu_p \sin\alpha\,(-1)^n$ (the f_s FID signal); at $\alpha = 30\,\mathrm{mrad}$, $|m_x|_{\text{FID}} \approx 8.2 \times 10^{-17}\,\mathrm{J\,T^{-1}}$ (inj), $2.0 \times 10^{-17}\,\mathrm{J\,T^{-1}}$ (flat)

Other EIC species

Nucleus	I	$\mu\,(\mu_N)$	G
p	$1/2$	$+2.7928$	$+1.7928$
d	1	$+0.8574$	-0.1426
^{3}He	$1/2$	-2.1276	-4.1914

SQUID couples to rank-1 vector moment only: p, ^{3}He give a signal $\propto P$; deuteron's tensor p_{zz} is invisible.

Moments from [14]; ^{3}He follows the proton analysis with $G = -4.19$.

A polarized bunch is a macroscopic dipole; a small tip turns it into the f_s FID signal.

SQUID readout parameters

Parameter	Symbol	Value
Coupling efficiency	η	0.7
Array channels	N_{squids}	4
White flux noise	$S_\Phi^{1/2}$	$0.4\,\mu\Phi_0/\sqrt{\mathrm{Hz}}$
Operating temp.	T	4 K

Magnicon-class two-stage sensor with XXF-1 electronics [15].

Noise floor and axial headroom

- On a 40-mm coil the single-bunch noise floor $\sim 1 \times 10^{-14}$ T (per-bunch $\mathrm{BW} \sim 1/\sigma_t \sim 1\,\mathrm{GHz}$). Along z-axis the dipole field falls as $1/z^3$, down to $\sim 1 \times 10^{-19}$ T by $z = 10\,\mathrm{cm}$, five orders below that floor
- The former can be extended axially at no signal cost, leaving room for a graded shield ($300 \to 40 \to 4\,\mathrm{K}$) within a $\sim 1\,\mathrm{W}$ pulse-tube cryocooler
- Architecture gains: $\sqrt{N_{\text{squids}}}$ in SNR; the polarization enters later as $P_\perp = P \sin\alpha$

Conservative, commercially available DC SQUID parameters: the sensitivity budget uses no exotic hardware.

SQUID basics

- A SQUID is a superconducting magnetometer reading flux in units of the flux quantum:

$$\Phi_0 = \frac{h}{2e} = 2.07 \times 10^{-15}\,\mathrm{Wb}$$

- Its noise is a spectral density, $S_\Phi^{1/2} \approx 0.4\,\mu\Phi_0/\sqrt{\mathrm{Hz}}$ at 4 K
- Polarized bunch couples $\sim 10^3\,\mu\Phi_0$ per pass in a sub-ns pulse; its single-shot noise over full band:

$$\mathrm{BW} \sim 1/\sigma_t \sim 1\,\mathrm{GHz}$$
$$\sigma_\Phi \approx S_\Phi^{1/2}\sqrt{\mathrm{BW}} \sim 10^4\,\mu\Phi_0$$

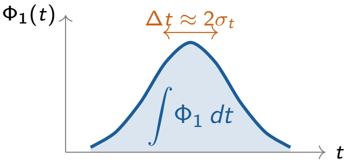

Per-pass pulse $\Phi_1(t)$; area $\widetilde{\Phi}_1 = \int \Phi_1\, dt$, boost-invariant.

- Signal below the single-shot noise; many turns summed coherently recover it, linear in P:

$$\mathrm{SNR}(T) = K_{\mathrm{template}}\, P_\perp \sqrt{T}$$
$$P_\perp = P \sin\alpha$$

Flux in units of Φ_0; a single bunch sits below the GHz-band noise, recovered by the matched filter as a signal linear in P.

Relativistic field of a moving dipole: flux per pass ▸ derivation ▸ integral

- Transverse dipole field at a coil at radius $r_{\rm coil}$:

$$\boxed{B_x^{\rm lab} = +\frac{\mu_0}{4\pi}\,\frac{2\,m_x}{r_{\rm coil}^3}}$$

- Boost compresses pulse to $\Delta t \approx 2\sigma_t \approx 0.40\,$ns (flattop), too brief for the time domain
- Flux per single saddle winding ($P = 1$): $\Phi_{\rm bunch} \approx 17.6\,\mu\Phi_0$ (inj), $4.41\,\mu\Phi_0$ (flat)
- With $N_{\rm turns} = 100$ windings and flux-transformer coupling efficiency $\eta = 0.7$: $\Phi_{\rm pickup} \approx 1236\,\mu\Phi_0$ (inj), $309\,\mu\Phi_0$ (flat) at the SQUID input

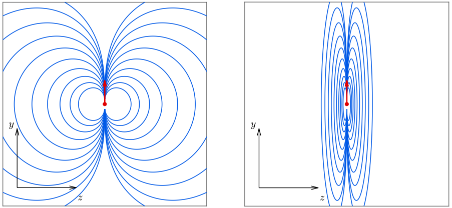

Dipole field in the y-z plane, rest (left) vs boosted (right, $\beta = 0.98$): longitudinal compression.

Peak γ-enhanced, but flux integral $\widetilde{\Phi}_1 = \int \Phi_1\,dt$ $(\propto \int B_x^{\rm lab}\,dz)$ is boost-invariant: amplitude γ cancels $1/\gamma$ compression, so $\gamma = 1$.

Peak γ-enhanced, flux integral boost-invariant: $\gamma = 1$ in the template: the per-pass numbers unchanged.

Bunch patterns and the matched filter ▸ coherent sum

- Injection sign pattern s_j: alternating bunch polarization $(-1)^j$, or random; fixed through the store. At flattop each parent splits into four daughters of the same sign
- Deterministic lattice phase from bunch position: $\psi_j = 2\pi\nu_s\, j/N_{\text{fill}} = \pi j/N_{\text{fill}}$ ($N_{\text{fill}} = 290$, 1160)
- A naive sum cancels: $C_{\text{naive}} \approx 1$ (inj), 4 (flat), discarding the whole multi-bunch gain

$$\boxed{w_j = s_j\, e^{-i\psi_j}}$$

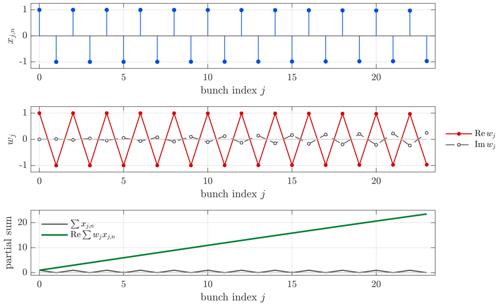

Raw samples carry s_j, ψ_j and the $(-1)^n$ turn factor; the weight w_j corrects them so the sum builds coherently.

Applying w_j aligns every bunch in phase; the sum then grows with N_{fill}.

Known sign and lattice phase turn a cancelling sum into coherent multi-bunch gain.

The FID protocol: tip, then free precession

The tipping kick

- In steady state spins lie along $\vec{n}_0 \simeq \vec{e}_y$; the $\cos\theta$ channel sees nothing until they are tipped
- A longitudinal B_z ($\parallel \vec{\beta}$, so no orbit kick) rotates them by α:

$$\boxed{\alpha = \frac{1+G}{B\rho} \int B_z \, dl}$$

The free-induction decay

- Free precession at f_s; $\nu_s = 1/2$ flips it each turn: $m_x^{\mathrm{FID}}(n) = PN_p\mu_p \sin\alpha\,(-1)^n$
- Impulsive if short against $T_s = 1/f_s \approx 25.6\,\mu\text{s}$: a sub-$\mu$s to few-$\mu$s solenoid or RF Wien-filter kick
- In tip, read, restore the polarization cost is set by the restore accuracy, not by α

Small longitudinal kick launches a freely precessing transverse moment, the FID, read at f_s.

Spectral search: signal out of the noise

- Each record spans one coherence window ($T_{\mathrm{meas}} = \tau_{\mathrm{coh}} \approx 2.04\,\mathrm{ms}$); the FID decays on its envelope (a) and noise buries it, $\mathrm{SNR}_1 \approx 1.2$ (b,c)
- Averaging N power spectra makes the f_s peak emerge as $\sqrt{N} = \sqrt{T_{\mathrm{tot}}/\tau_{\mathrm{coh}}}$, reaching $\sim 36\sigma$ in $\sim 1.7\,\mathrm{min}$ (d)

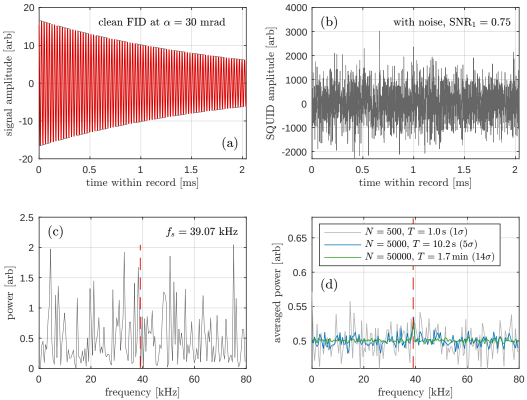

Injection: (a) clean FID with its coherence envelope, (b) same buried in SQUID noise, (c) one spectrum, (d) f_s peak after N averages.

Spin coherence time sets the record length; the precession peak is recovered by stacking many coherence-limited records ($\propto \sqrt{N}$).

Spectral search: ν_s and σ_{ν_s} from the SQUID alone ▸ diagnostic

- One cycle: tip ($\alpha = 30\,\mathrm{mrad}$), record the FID for $T_\mathrm{meas} \leq \tau_\mathrm{coh}$, FFT, restore; repeat N times and average the power spectra incoherently
- Peak position $\to \nu_s$; peak width $\to \sigma_{\nu_s}$ through $\tau_\mathrm{coh} = 1/(2\pi f_\mathrm{rev}\sigma_{\nu_s})$
- 10σ in $\lesssim 1\,\mathrm{s}$ (inj), $\sim 20\,\mathrm{s}$ (flat); since $T_\mathrm{tot} \propto \sigma^2_{\nu_s}$, a $10\times$ better lattice is $100\times$ faster

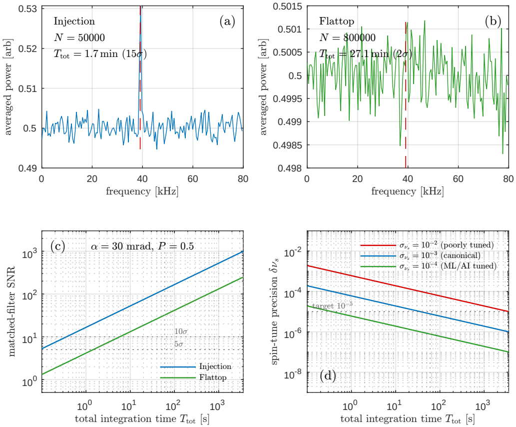

Averaged spectra at both energies, $\sqrt{T_\mathrm{tot}}$ significance scaling, and the σ_{ν_s} dependence of the precision.

One non-invasive search returns ν_s and coherence diagnostic σ_{ν_s}, then feeds lattice tuning.

Two coherence times: T_2^* and T_2 ▸ linewidth table

Reversible: T_2^*

- Spin-tune spread σ_{ν_s} (off-momentum, betatron amplitude) fans the transverse phases
- FID envelope decays with $T_2^* = \tau_{\mathrm{coh}} = 2.04\,\mathrm{ms}$ ($\sigma_{\nu_s} = 10^{-3}$); linewidth $\sigma_f \simeq f_{\mathrm{rev}}\sigma_{\nu_s} \approx 78\,\mathrm{Hz}$
- Deterministic in each spin frequency, so a pulse can undo it

$$\boxed{T_2^* = \frac{1}{2\pi f_{\mathrm{rev}}\,\sigma_{\nu_s}}}$$

Irreversible: T_2

- Processes that change individual spin tunes mid-measurement: intra-bunch scattering, orbit and snake drift, residual gas, beam losses
- A random walk in phase that no pulse can undo; $T_2 \gg T_2^*$ sets the ultimate signal envelope
- The spin echo separates the two and measures T_2 directly

Reversible T_2^* from spread, irreversible T_2 from diffusion; the echo tells them apart.

Spin echo: a π pulse rephases the ensemble

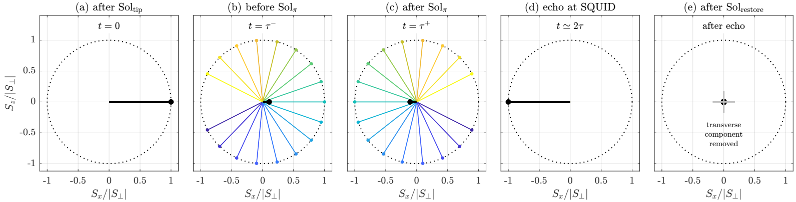

Rotating-frame phase fan: tip, fan-out, π reflection, rephasing echo, restore.

- Hahn echo: a coherent π pulse at $t=\tau$ reflects the fan, which rephases at $t=2\tau$
- π about $\vec{e}_z$, the kicker's own axis: $R_z(\pi):(S_x,S_y,S_z)\to(-S_x,-S_y,S_z)$
- At 2τ all particles re-align at $(\sin\alpha,-\cos\alpha,0)$, independent of $\delta\nu_s$
- T_2^* cancels; a τ-scan of the echo gives T_2

$$\boxed{\frac{M_\perp(2\tau)}{M_\perp(0)}=e^{-2\tau/T_2}}$$

π pulse folds spread-out spins back into an echo, exposing true irreversible decoherence T_2.

The closed tip, π, echo, restore cycle ▸ π-pulse fields

- One longitudinal kicker delivers all four pulses (tip, π, echo readout by SQUID, restore), phase-locked to f_s
- Restore $R_z(\pi - \alpha)$ returns the ensemble to $(0, 1, 0)$ at a cost $\mathcal{O}(\alpha^2/\pi^2) \sim 10^{-4}$ per cycle
- A single-shot π would need $\int B_z\, dl \approx 88\,\mathrm{T\,m}$ (inj), $1032\,\mathrm{T\,m}$ (flat); spread over $N \leq 1/(4\pi\sigma_{\nu_s}) \approx 80$ synchronized passes it falls to a feasible $1.1\,\mathrm{T\,m}$ (inj), $12.9\,\mathrm{T\,m}$ (flat) per pass
- Repeated through an ∼8-hour fill: continuous f_s, σ_{ν_s}, and in-plane P with negligible depletion, a train of π (refocusing) pulses (CPMG) removes drift

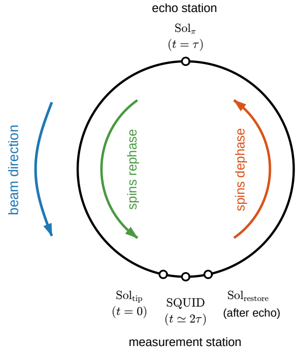

One station: the longitudinal kicker delivers tip, π, and restore; the SQUID samples the echo near $t \simeq 2\tau$. All pulses are locked to the reference at f_s.

Closed cycle preserves polarization, turning polarimetry into continuous, non-invasive monitoring.

What the SQUID sees: the echo τ-scan

- Across one cycle the coherent envelope decays on T_2^*, π pulse at $t = \tau$ reverses fan, and the echo peaks near $t = 2\tau$, reduced by $e^{-2\tau/T_2}$
- The spin precession at $f_s \approx 39.1\,\mathrm{kHz}$ continues throughout: the echo restores the slow envelope, not the precession
- A τ-scan of the echo amplitude gives T_2; the FID linewidth in the same record gives T_2^*
- Both coherence times from one fill; the ratio T_2/T_2^* separates recoverable dephasing from genuine loss

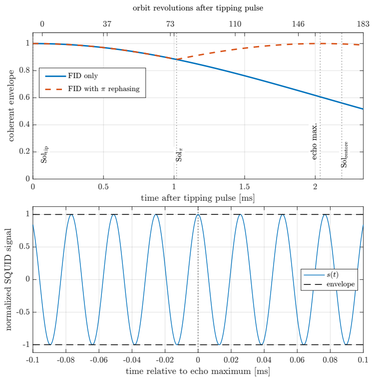

Upper: transverse-spin envelope (FID decay, π at τ, echo near 2τ). Lower: zoom near echo, f_s precession continuing through sequence.

One continuous record yields both T_2 (echo τ-scan) and T_2^* (FID linewidth): a built-in coherence diagnostic.

Matched-filter sensitivity

- Coherent integration over time T gives a linear-in-P signal-to-noise ratio ($P_\perp = P \sin\alpha$):

$$\boxed{\mathrm{SNR}(T) = K_{\mathrm{template}}\, P_\perp \sqrt{T}}$$

- $K_{\mathrm{template}} = \dfrac{\Phi_{\mathrm{pickup}}}{S_\Phi^{1/2}} \sqrt{N_{\mathrm{fill}}\, f_{\mathrm{rev}}\, \tau_h\, N_{\mathrm{squids}}}$
- effective pulse width $\tau_h = \sqrt{\pi}\, \sigma_t$
- Four factors: flux-to-noise $\Phi_{\mathrm{pickup}}/S_\Phi^{1/2}$; statistics $\sqrt{N_{\mathrm{fill}} f_{\mathrm{rev}}}$; matched window $\sqrt{\tau_h}$; array $\sqrt{N_{\mathrm{squids}}}$

Hardware-fixed scale

K [$\mathrm{s}^{-1/2}$]	injection	flattop
Saddle (P_x, P_y)	1108	277
Axial (P_z)	156.8	198.4

- Injection beats flattop $\times 4$ on the saddle: N_p enters Φ_{pickup} linearly, N_{fill} only as $\sqrt{N_{\mathrm{fill}}}$

Sensitivity factorizes into hardware $\times$ statistics; the fixed scale K reaches $\sim 1100\ \mathrm{s}^{-1/2}$ at injection.

Integration times to $\delta P/P = 1\%$

- $P_\perp = P \sin\alpha \approx 0.021$ ($P = 0.7$, $\alpha = 30\,\mathrm{mrad}$); $T_{1\%} = (100/K_{\mathrm{template}} P_\perp)^2$

Case	Analysis	$T_{1\%}$
Inj, 290	naive	18 days
Inj, 290	same-sign	73.9 s
Inj, 290	matched	18.5 s
Flat, 1160	naive	288 days
Flat, 1160	matched	4.93 min

At full projection ($\sin\alpha = 1$): 6.5 ms (inj), 104 ms (flat); the $1/\sin^2\alpha$ penalty buys non-invasiveness.

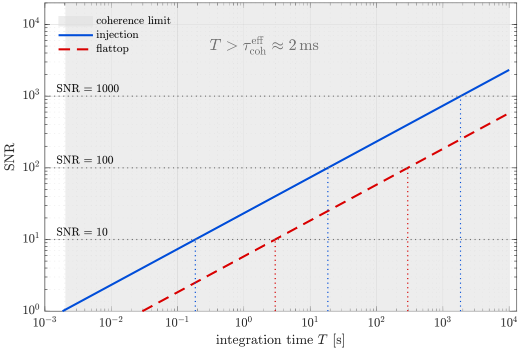

Matched-filter SNR vs T at both energies; dotted lines mark SNR $= 10, 100, 1000$ ($10\%, 1\%, 0.1\%$). Grey: $T > \tau_{\mathrm{coh}} \simeq 2.04\,\mathrm{ms}$, handled as repeated cycles.

Matched filter reaches 1% in $\sim$18 s (inj) and $\sim$5 min (flat); mm tip angle, not hardware, sets clock.

Optimization headroom

Sensitivity scales with the hardware as

$$K_{\text{template}} \propto \frac{\eta\,\sqrt{N_{\text{squids}}}}{S_{\Phi}^{1/2}}$$

Three modest, independent upgrades, each within current practice:

- flux noise $S_{\Phi}^{1/2}$: $0.4 \to 0.3\ \mu\Phi_0/\sqrt{\mathrm{Hz}}$ (multi-stage arrays, sub-K operation)
- coupling η : $0.7 \to 0.9$ (inductive matching)
- channels N_{squids} : $4 \to 8$

Compound effect

- Together $K_{\text{template}} \mapsto 2.4\,K_{\text{template}}$: a $\sim 6\times$ shorter integration at fixed precision
- Optimized 1% times: $\sim 3\,\mathrm{s}$ (inj), $\sim 50\,\mathrm{s}$ (flat)
- This bounds the practical performance ceiling of the baseline architecture

Three off-the-shelf upgrades compound to $2.4\times$ *sensitivity,* $\sim 6\times$ *faster:* 1% *in a few seconds at injection.*

Static vector mode: reading $\vec{P}$ without tipping

- In steady state each channel reads a definite component of $\vec{m} = N_p \mu_p \vec{P}$; the time structure comes from the bunch passage, not from any spin manipulation
- Arc pickup ($\vec{n}_0 \simeq \vec{e}_y$): stored P_y gives m_y steady on the precession scale, pulsing at f_{rev}
- Residual P_x, P_z oscillate at $f_s = f_{\mathrm{rev}}/2$, alternating bunch to bunch; the three symmetry classes separate them

Beam-synchronous reconstruction

- Pulse train: $\vec{\Phi}^{\mathrm{m}}(t) = \sum_{n,b} \mathrm{H}(t - t_{n,b})\, c_b\, \vec{m}_b + \vec{B}^{\mathrm{bg}}$
- Three simultaneous matched filters, one per channel:

$$\hat{m}_i \propto \sum_{n,b} \int dt\, \Phi^{\mathrm{m}}_i(t)\, q_i(t - t_{n,b})\, c_b$$

- Read simultaneously or interleaved: either way a quasi-continuous $\vec{P}(t)$

No tipping needed: the known bunch pattern lets three matched filters reconstruct (P_x, P_y, P_z) continuously.

Angular pickup basis on the cylinder

convolution

- The field of a magnetic dipole on the cylinder (radius r_{coil}) produces radial fields in three angular classes:

$$\boxed{B_r^{(x)} \propto \cos\phi, \quad B_r^{(y)} \propto \sin\phi, \quad B_r^{(z)}: \ \text{axial}}$$

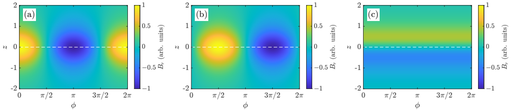

Unwrapped cylinder (ϕ horizontal, z vertical): (a) $\cos\phi$ (m_x), (b) $\sin\phi$ (m_y), (c) axial (m_z).

- Orthogonality ($\int \cos\phi \sin\phi \, d\phi = \int \cos\phi \, d\phi = 0$) makes the transverse channels mutually orthogonal and blind to symmetric fields

- The axial response is ϕ-independent, a distinct symmetry class, so it carries m_z without transverse leakage

Each component lives in its own angular symmetry class, so the basis separates $\vec{P}$ and rejects the symmetric charge field.

Cross-talk and systematics: a calibration program

In ideal apparatus, channels are orthogonal (diagonal response); real winding errors, conductive structures, and shared routing add off-diagonal cross-talk R_{ij} ($\hat{m}_i = \sum_j R_{ij} P_j + B_i^{\mathrm{bg}}$). A centered beam has no $m = 1$ image-current term, so the $\cos\theta$ and $\sin\theta$ windings reject it, leaving only higher multipoles [16]. Calibration fixes R_{ii} and bounds R_{ij}.

Category	Origin	Suppression or calibration
Geometric cross-talk	Winding errors, layer offsets, tilt	Survey, bench calibration, response matrix
Charge-current leakage	Broken symmetry, image currents	Gradiometry, trim coils, shielding
Environmental	External fields, vibration, trapped flux	SC shield, quiet location, cooldown
Spin-correlated	Machine or bunch-pattern correlations	Pattern reversal, bunch-subset tests, HJET/pC
Gain and phase	SQUID, FLL, electronics	Injected calibration, RF-clock reference

Cross-talk is engineering limit, not fundamental one: response-matrix calibration plus listed strategies.

Axial gradiometer: geometric charge rejection

Charge-blind by geometry

- Beam's charge current purely azimuthal, a coaxial loop (normal $\parallel \vec{e}_z$) is threaded only by B_z:

$$\boxed{\Phi_{\text{charge}} = \oint \vec{B}_{\text{charge}} \cdot d\vec{A} = 0 \quad \text{exactly}}$$

- Exact at all frequencies and any beam profile, with no winding balance, unlike the $\cos\theta$ coil, which needs a common-mode rejection ratio $\mathrm{CMRR} = 1/\epsilon \gtrsim 10^{12}$ (ϵ: winding imbalance)

Gradiometer pair

- Two coaxial loops in series opposition ($\Delta z = 30\,\text{cm}$): cancel uniform B_z, keep the bipolar bunch pulse, and retain $\sim$65% of the single-loop peak
- Peak flux to SQUID: $174.9\,\mu\Phi_0$ (inj), $221.3\,\mu\Phi_0$ (flat): 14% and 72% of $\cos\theta$ coil

By geometry the coaxial loop sees no charge-current field; the gradiometer pair adds uniform-field rejection.

Axial channel sensitivity

- Per-bunch flux is well below the floor; recovered by coherent summation at the f_s sideband, $\mathrm{SNR} \propto \sqrt{T}$:

$$\boxed{\mathrm{SNR}_z^{(1)}(T) = \frac{\Phi_z^{\mathrm{peak}} \sqrt{N_b\, f_{\mathrm{rev}}\, T}}{S_\Phi^{1/2}}}$$

- Strategy 1 (all bunches): the sensitivities K_z below
- Strategy 2 (single tagged bunch): lower by $\sqrt{N_b}$ (≈ 17 at injection), but gives bunch-resolved $\vec{P}(t)$; $T > \tau_{\mathrm{coh}}$ runs as echo cycles, as for the saddles

	injection	flattop
K_z [$\mathrm{s}^{-1/2}$]	156.8	198.4
Φ_z/Φ_x	0.142	0.716

- Weaker than $\cos\theta$ at injection; the short flattop bunch ($\sigma_L \simeq r_{\mathrm{coil}}$) nearly closes the gap
- $T_{1\%}$ for an assumed residual P_z (0.03 inj, 0.10 flat, anchored on pC tilt data [17]): 7.53 min (inj), 25.4 s (flat)

> *The axial channel trails the saddles at injection but nearly matches them at flattop; the echo extends it past τ_{coh}.*

What P_z buys, and what is left for engineering

Why measure P_z

- It completes the spin vector: the saddles cannot see m_z, so the gradiometer is what makes this a true three-component polarimeter
- A non-zero P_z flags snake and rotator transients, injection mismatch, and resonance crossings, anchored on the RHIC pC transverse-tilt observations [17]
- Minimal hardware: two NbTi loops on same former ($r_{\mathrm{coil}} = 40\,\mathrm{mm}$, $\Delta z = 30\,\mathrm{cm}$) and one extra wideband SQUID channel, no cryostat change

Open items for a design paper

- Loop-tilt tolerance (the only misalignment that breaks the exact charge rejection)
- Image currents and Cu coating ($50\,\mu\mathrm{m}$ to $100\,\mu\mathrm{m}$ skin-depth guide), non-uniform B_z leakage, inter-channel cross-talk
- Absolute scale: cross-calibrate against the HJET standard [1]

P_z completes the three-component vector polarimeter using two circular NbTi loops and one SQUID channel; the rest is engineering, anchored by HJET calibration.

Three-channel modes, and what only the SQUIDs provide

Static mode reads all three components at their natural frequencies; dynamic mode fires the kicker for α calibration.

comp.	mode	channel (f)	$T_{1\%}$ inj	$T_{1\%}$ flat
P_y	static	sin-θ (f_{rev})	16.6 ms	266 ms
P_x	static	cos-θ (f_s)	9.05 s	13 s
P_z	static	axial (f_s)	7.53 min	25.4 s
P_y	dynamic	cos-θ (f_s)	18.5 s	4.93 min
P_x	dynamic	sin-θ (f_{rev})	2.79 h	4.03 h
P_z	dynamic	sin-θ (f_{rev})	2.79 h	4.03 h

- pC: blind to P_z by selection rule (parity-violating analyzing power, zero under strong interaction)
- HJET: reaches P_z only with a dedicated longitudinal target, slow and fill-averaged
- SQUID: senses m_z directly, continuous and bunch-resolved

Static mode reads all three components continuously; only the SQUID delivers P_z, bunch by bunch.

Bunch-resolved polarization history

- Full $\vec{P}(t)$ for every bunch, continuously and non-invasively across the fill
- Synthetic 8-hour flattop fill ($N_b = 1160$): P_y slow decay (a); residual P_x (b) and P_z (c) with drifts and two localized anomalies
- Panel (c) shows bunch-resolved longitudinal reconstruction, beyond reach of pC and HJET; per-bunch costs only $\sqrt{N_b} \approx 34$ vs all-bunch (180 s gives $\sim$1%, 160 time bins per fill)

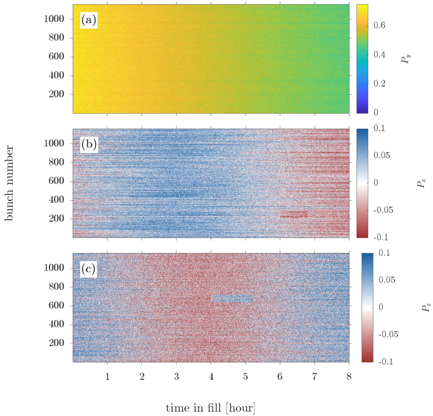

Heatmaps 8-hour fill: (a) dominant P_y, (b) residual P_x, (c) residual P_z (first-ever bunch-resolved).

SQUIDs able to map full spin vector for every bunch through store, resolving drifts and anomalies, including first bunch-resolved P_z.

Extensions and outlook ▸ Wien filter

Beyond proton polarimetry

- Same pickup for deuteron and ^{3}He via species spin-magnetic factors; supports storage-ring EDM and BSM programs (follow-up)

Bunch-gated spin control

- An orbit-preserving RF Wien filter reverses polarization bunch by bunch (COSY: per-flip $\varepsilon_{\mathrm{SF}} = 0.9954$ [18])
- Paired with bunch-resolved readout: per-bunch (P_x, P_y, P_z) and per-bunch reversal ($\nu_s = 1/2$ needs rotation-sense selection)

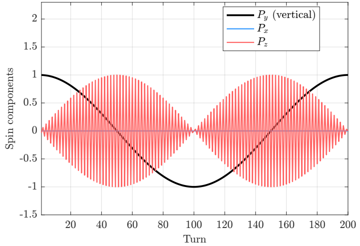

Resonant RF Wien filter (turn by turn): P_y reverses, P_z oscillates, P_x stays constant, a coherent rotation about the radial axis.

> *The concept extends to d and ^{3}He and to EDM/BSM programs; an RF Wien filter adds per-bunch spin control.*

Outlook: a SQUID readout for storage-ring EDM searches

Frozen-spin EDM rings

- Light ions at the magic momentum $p_{\mathrm{magic}} = mc/\sqrt{G} \approx 0.70\ \mathrm{GeV}/c$ (p) freeze the in-plane $g-2$ precession (spin tracks velocity)
- An EDM tilts the spin out of plane: a tiny vertical polarization $P_y(t)$ grows almost linearly, the signal
- Counter-propagating CW and CCW beams cancel the dominant fake-EDM systematic (radial B fields)

Why the SQUID fits

- The signal is a slowly growing out-of-plane moment, exactly what the static vector and axial channels read
- Non-destructive and continuous: read both beams in real time, replacing slow destructive scattering polarimetry
- The CW$-$CCW difference isolates the EDM; the ring's stable f_{rev} enables coherent integration

Frozen-spin rings store counter-propagating light ions at the magic momentum, and their EDM signal is a slowly growing out-of-plane moment: a natural, continuous target for SQUID polarimetry, and a dedicated follow-up.

Outlook: electrons and a stable revolution frequency

Sokolov-Ternov

The ESR is the natural fit

- A storage ring with a stable f_{rev}: the matched filter and FID echo phase up over many turns, as in the HSR
- $\mu_e/\mu_p \approx 658$ plus a tighter coil give orders of magnitude more flux; integration $\propto \Phi_{\mathrm{pickup}}^{-2}$ collapses to ms
- Spin dynamics differ: Sokolov-Ternov is fast and spin-state-asymmetric, bunches against the guide field decay faster than the aligned ones ($\tau_{\mathrm{ST}} \sim$ min at 18 GeV, $\propto E^{-5}$); $\nu_s = a_e\gamma \approx 41$, no snake $\frac{1}{2}$

Ramping or recirculating: not direct users

- The coherent sum needs a stable, long-lived revolution period to predict the turn-by-turn phase
- RCS: the fast ramp leaves no stable f_{rev} and ν_s sweeps through resonances, so there is no coherent window
- JLab CEBAF: a recirculating linac has no revolution frequency at all; at best single-pass detection, aided by the large moment

Coherent integration needs a stable f_{rev}: the ESR is the natural electron home, while the rapidly ramping RCS and the recirculating JLab linac are not direct users.

Outlook: the spin tune as a precision machine diagnostic

◂ ν_s readout

- The same readout that yields $\vec{P}$ also gives the spin tune, from the precession phase tracked over many turns.
- ν_s near 1/2; the spin-tune response diagnoses, non-invasively:
  - snake setting
  - spin matching
  - imperfection fields

- Demonstrated at COSY (JEDI):
  - continuous spin-tune readout to order 10^{-8} in 2.6 s and 1×10^{-10} over a 100 s cycle, among the most precise quantities in any accelerator [2]
  - spin-tune mapping determined the stable spin axis $\vec{n}_0$ to better than 2.8 μrad and exposed imperfection fields [3]

> *Read continuously, the spin tune turns the polarimeter into a fine-grained, non-invasive probe of the machine itself: real-time feedback for spin and orbit tuning.*

Conclusions

- On the six-snake $\nu_s = 1/2$ HSR, a SQUID reads the bunch magnetic moment at $f_s = f_{\mathrm{rev}}/2$; three channels ($\cos\theta$, $\sin\theta$, axial) give all three projections (P_x, P_y, P_z) at one station, built up over many turns.
- Phase-locked tip-π-echo-restore cycles return the spin to $\vec{n}_0$, so the polarization cost is negligible: truly non-invasive
- $K_{x,y} \approx 1108$ (inj), 277 (flat); $K_z \approx 156.8$ (inj), 198.4 (flat), in $\mathrm{s}^{-1/2}$; static 1% times from $\sim$17 ms to $\sim$7.5 min, all under 30 s at flattop
- Continuous, bunch-resolved $\vec{P}(t)$ for every bunch; P_z becomes a routine observable (first bunch-resolved longitudinal), plus a spin-tune and coherence diagnostic
- A conservative baseline: three modest upgrades compound to $2.4 \times K$, about $6\times$ faster
- Feasible with currently available SQUID technology

Non-invasive, bunch-resolved, three-component polarimetry of the EIC proton beam, including the longitudinal P_z, is feasible today.

Thank you

Questions and discussion welcome

"There is a goal, but no way;
what we call a way is hesitation."

Es gibt ein Ziel, aber keinen Weg;
was wir Weg nennen, ist Zögern.

Franz Kafka, *Die Zürauer Aphorismen*, no. 26

References

[1] F. Rathmann, A. Nass, K. O. Eyser, V. Shmakova, E. C. Aschenauer, G. Atoian, A. Cannavo, X. Chu, K. Hock, H. Huang, H. Lovelace, G. Mahler, N. N. Nikolaev, J. Ritter, G. Robert-Demolaize, V. Schoefer, P. Shanmuganathan, E. Shulga, H. Soltner, and Z. Zhang. Eliminating beam-induced depolarizing effects in the hydrogen jet target for high-precision proton beam polarimetry at the electron-ion collider. *Phys. Rev. Accel. Beams*, 29:021001, Feb 2026. URL: https://link.aps.org/doi/10.1103/8nh5-163q, doi:10.1103/8nh5-163q.

[2] D. Eversmann, V. Hejny, F. Hinder, A. Kacharava, J. Pretz, F. Rathmann, M. Rosenthal, F. Trinkel, S. Andrianov, W. Augustyniak, Z. Bagdasarian, M. Bai, W. Bernreuther, S. Bertelli, M. Berz, J. Bsaisou, S. Chekmenev, D. Chiladze, G. Ciullo, M. Contalbrigo, J. de Vries, S. Dymov, R. Engels, F. M. Esser, O. Felden, M. Gaisser, R. Gebel, H. Glückler, F. Goldenbaum, K. Grigoryev, D. Grzonka, G. Guidoboni, C. Hanhart, D. Heberling, N. Hempelmann, J. Hetzel, R. Hipple, D. Hölscher, A. Ivanov, V. Kamerdzhiev, B. Kamys, I. Keshelashvili, A. Khoukaz, I. Koop, H.-J. Krause, S. Krewald, A. Kulikov, A. Lehrach, P. Lenisa, N. Lomidze, B. Lorentz, P. Maanen, G. Macharashvili, A. Magiera, R. Maier, K. Makino, B. Mariański, D. Mchedlishvili, Ulf-G. Meißner, S. Mey, A. Nass, G. Natour, N. Nikolaev, M. Nioradze, A. Nogga, K. Nowakowski, A. Pesce, D. Prasuhn, J. Ritman, Z. Rudy, A. Saleev, Y. Semertzidis, Y. Senichev, V. Shmakova, A. Silenko, J. Slim, H. Soltner, A. Stahl, R. Stassen, M. Statera, E. Stephenson, H. Stockhorst, H. Straatmann, H. Ströher, M. Tabidze, R. Talman, P. Thörngren Engblom, A. Trzciński, Yu. Uzikov, Yu. Valdau, E. Valetov, A. Vassiliev, C. Weidemann, C. Wilkin, A. Wirzba, A. Wrońska, P. Wüstner, M. Zakrzewska, P. Zuprański, and D. Zyuzin. New method for a continuous determination of the spin tune in storage rings and implications for precision experiments. *Phys. Rev. Lett.*, 115:094801, Aug 2015. URL: https://link.aps.org/doi/10.1103/PhysRevLett.115.094801, doi:10.1103/PhysRevLett.115.094801.

[3] A. Saleev, N. N. Nikolaev, F. Rathmann, W. Augustyniak, Z. Bagdasarian, M. Bai, L. Barion, M. Berz, S. Chekmenev, G. Ciullo, S. Dymov, D. Eversmann, M. Gaisser, R. Gebel, K. Grigoryev, D. Grzonka, G. Guidoboni, D. Heberling, V. Hejny, N. Hempelmann, J. Hetzel, F. Hinder, A. Kacharava, V. Kamerdzhiev, I. Keshelashvili, I. Koop, A. Kulikov, A. Lehrach, P. Lenisa, N. Lomidze, B. Lorentz, P. Maanen, G. Macharashvili, A. Magiera, D. Mchedlishvili, S. Mey, F. Müller, A. Nass, A. Pesce, D. Prasuhn, J. Pretz, M. Rosenthal, V. Schmidt, Y. Semertzidis, Y. Senichev, V. Shmakova, A. Silenko, J. Slim, H. Soltner, A. Stahl, R. Stassen, E. Stephenson, H. Stockhorst, H. Ströher, M. Tabidze, G. Tagliente, R. Talman, P. Thörngren Engblom, F. Trinkel, Yu. Uzikov, Yu. Valdau, E. Valetov, A. Vassiliev, C. Weidemann, A. Wrońska, P. Wüstner, P. Zupráński, and M. Zurek. Spin tune mapping as a novel tool to probe the spin dynamics in storage rings. *Phys. Rev. Accel. Beams*, 20:072801, Jul 2017. URL: https://link.aps.org/doi/10.1103/PhysRevAccelBeams.20.072801, doi:10.1103/PhysRevAccelBeams.20.072801.

References

[4] C. Liu, J. Kewisch, H. Huang, and M. Minty. Minimization of spin tune spread for preservation of spin polarization at rhic. *Phys. Rev. Accel. Beams*, 22:061002, 2019. doi:10.1103/PhysRevAccelBeams.22.061002.

[5] Brookhaven National Laboratory / Jefferson Lab. EIC global system requirements, 2022. URL: https://eic.jlab.org/Requirements/GLOBAL.html.

[6] F. Rathmann, B. von Przewoski, W. A. Dezarn, J. Doskow, M. Dzemidzic, W. Haeberli, J. G. Hardie, B. Lorentz, H. O. Meyer, P. V. Pancella, R. E. Pollock, T. Rinckel, F. Sperisen, and T. Wise. Complete angular distribution measurements of pp spin correlation parameters A_{xx}, A_{yy}, and A_{xz} and analyzing power A_y at 197.4 mev. *Phys. Rev. C*, 58:658–673, Aug 1998. URL: https://link.aps.org/doi/10.1103/PhysRevC.58.658, doi:10.1103/PhysRevC.58.658.

[7] V. Schoefer, E.C. Aschenauer, H. Huang, F. Mèot, V. Ptitsyn, and V. H. Ranjbar. Stable spin direction measurements at RHIC with polarized proton beams. Technical Report BNL-225293-2024-TECH C-A/AP/703, Brookhaven National Laboratory, January 2024.

[8] P. R. Cameron, A. U. Luccio, T. J. Shea, and D. A. Goldberg. Squids, snakes, and polarimeters: A new technique for measuring the magnetic moments of polarized beams. In *High Energy Spin Physics: 12th International Symposium*, volume 390 of *AIP Conference Proceedings*, pages 306–315. American Institute of Physics, 1997. doi:10.1063/1.51839.

[9] Eiad Hamwi and Georg H. Hoffstaetter. Polarization transmission in the Electron-Ion Collider's Hadron Storage Ring. 2025. URL: https://arxiv.org/abs/2509.18558, arXiv:2509.18558.

[10] V. Bargmann, L. Michel, and V. L. Telegdi. Precession of the polarization of particles moving in a homogeneous electromagnetic field. *Phys. Rev. Lett.*, 2:435, 1959. doi:10.1103/PhysRevLett.2.435.

[11] V. Ptitsyn and J. S. Berg. EIC hadron spin rotators. In *Proc. 13th International Particle Accelerator Conference (IPAC2022)*, pages 1734–1736, Geneva, Switzerland, 2022. JACoW Publishing. Paper WEPOST020. URL: https://proceedings.jacow.org/ipac2022/papers/wepost020.pdf, doi:10.18429/JACoW-IPAC2022-WEPOST020.

References

[12] N. Hempelmann et al. Phase measurement for driven spin oscillations in a storage ring. *Phys. Rev. Accel. Beams*, 21:042002, 2018. doi:10.1103/PhysRevAccelBeams.21.042002.

[13] P. J. Mohr, D. B. Newell, and B. N. Taylor. CODATA recommended values of the fundamental physical constants: 2014. *Rev. Mod. Phys.*, 88:035009, 2016. doi:10.1103/RevModPhys.88.035009.

[14] N. J. Stone. Table of nuclear magnetic dipole and electric quadrupole moments. *At. Data Nucl. Data Tables*, 111–112:1–28, 2016. doi:10.1016/j.adt.2015.12.002.

[15] D. Drung, C. Abmann, J. Beyer, A. Kirste, M. Peters, F. Ruede, and Th. Schurig. Highly sensitive and easy-to-use squid sensors. *IEEE Transactions on Applied Superconductivity*, 17(2):699–704, 2007. doi:10.1109/TASC.2007.897403.

[16] D. Xu et al. EIC beam dynamics challenges. Technical Report Fermilab-Conf-22-682-AD, Fermilab, 2022. URL: https://lss.fnal.gov/archive/2022/conf/fermilab-conf-22-682-ad.pdf.

[17] W. B. Schmidke. RHIC polarization for Runs 9–17. Technical Report BNL-209057-2018-TECH, C-A/AP/609, Brookhaven National Laboratory, September 2018. URL: https://www.osti.gov/servlets/purl/1473643.

[18] J. Slim, F. Rathmann, A. Andres, V. Hejny, A. Nass, A. Kacharava, P. Lenisa, N. N. Nikolaev, J. Pretz, A. Saleev, V. Shmakova, H. Soltner, F. Abusaif, A. Aggarwal, A. Aksentev, B. Alberdi, L. Barion, I. Bekman, M. Beyß, C. Böhme, B. Breitkreutz, N. Canale, G. Ciullo, S. Dymov, N.-O. Fröhlich, R. Gebel, M. Gaisser, K. Grigoryev, D. Grzonka, J. Hetzel, O. Javakhishvili, V. Kamerdzhiev, S. Karanth, I. Keshelashvili, A. Kononov, K. Laihem, A. Lehrach, N. Lomidze, B. Lorentz, G. Macharashvili, A. Magiera, D. Mchedlishvili, A. Melnikov, F. Müller, A. Pesce, V. Poncza, D. Prasuhn, D. Shergelashvili, N. Shurkhno, S. Siddique, A. Silenko, R. Stassen, E. J. Stephenson, H. Ströher, M. Tabidze, G. Tagliente, Y. Valdau, M. Vitz, T. Wagner, A. Wirzba, A. Wrońska, P. Wüstner, and M. Żurek. Proof-of-principle demonstration of a pilot bunch comagnetometer in a stored beam. *Phys. Rev. Res.*, 7:023257, Jun 2025. URL: https://link.aps.org/doi/10.1103/PhysRevResearch.7.023257, doi:10.1103/PhysRevResearch.7.023257.

References

[19] S. Y. Lee and E. D. Courant. Tolerance of imperfections in high-energy circular accelerators for polarized protons. *Phys. Rev. D*, 41:292–302, Jan 1990. URL: https://link.aps.org/doi/10.1103/PhysRevD.41.292, doi:10.1103/PhysRevD.41.292.

[20] Eiad Hamwi. *Spin Polarization, Modeling, and Beam Control in Hadron Accelerators: For RHIC and the EIC*. Ph.d. dissertation, Cornell University, December 2025.

[21] C. F. von Weizsäcker. Ausstrahlung bei stößen sehr schneller elektronen. *Zeitschrift für Physik*, 88(9–10):612–625, 1934. doi:10.1007/BF01333110.

[22] E. J. Williams. Nature of the high energy particles of penetrating radiation and status of ionization and radiation formulae. *Phys. Rev.*, 45(10):729–730, 1934. doi:10.1103/PhysRev.45.729.

[23] M. Bai, T. Roser, C. Dawson, J. Kewisch, Y. Makdisi, P. Oddo, C. Pai, and P. Pile. Rhic spin flipper commissioning results. In *Proceedings of IPAC2012*, pages 1302–1304, New Orleans, Louisiana, USA, 2012. https://proceedings.jacow.org/IPAC2012/papers/tuppc057.pdf. URL: https://proceedings.jacow.org/IPAC2012/papers/tuppc057.pdf.

[24] A. A. Sokolov and I. M. Ternov. On polarization and spin effects in the theory of synchrotron radiation. *Sov. Phys. Dokl.*, 8:1203, 1964.

[25] D. Xu, F. Willeke, M. Blaskiewicz, Y. Luo, and C. Montag. Advancing electron injection dynamics and mitigation approaches in the EIC swap-out injection scheme. In *Proc. 15th Int. Particle Accelerator Conf. (IPAC'24)*, 2024. arXiv:2405.08712.

[26] Ya. S. Derbenev and A. M. Kondratenko. Polarization kinematics of particles in storage rings. *Sov. Phys. JETP*, 37:968, 1973. [Zh. Eksp. Teor. Fiz. **64**, 1918 (1973)].

[27] S. R. Mane. Electron-spin polarization in high-energy storage rings. I. derivation of the equilibrium polarization. *Phys. Rev. A*, 36:105, 1987. doi:10.1103/PhysRevA.36.105.

References

[28] S. R. Mane. Electron-spin polarization in high-energy storage rings. II. evaluation of the equilibrium polarization. *Phys. Rev. A*, 36:120, 1987. doi:10.1103/PhysRevA.36.120.

Backup slides

Supporting derivations, parameters, and , and numerical detail

Backup: parameters at a glance ◂ the idea

Beam (injection and flattop)

Parameter	inj	flat
Energy E (GeV)	23.5	275
Lorentz γ	25.05	293.1
β	0.9992	0.999994
Protons per bunch N_p (10^{10})	27.6	6.9
Bunches N_b	290	1160
Spacing T_b (ns)	44.1	11.0
RMS width σ_t (ns)	0.801	0.200
RMS length σ_L (m)	0.24	0.06
Current $I_{\rm avg}$ (A)	1.002	1.003
$f_{\rm rev}$ (kHz)	78.13	78.20

Constants and operating point

Parameter	Value
Circumference C	3833.85 m
Spin tune ν_s	0.5
Proton anomaly G	1.7928
Polarization P	0.70
Tipping angle α	30 mrad
Spread $\sigma_{\nu_s}^{\rm eff}$	10^{-3}
Spin freq $f_s = f_{\rm rev}/2$	39.1 kHz
Coherence $\tau_{\rm coh}^{\rm eff}$	2.04 ms

SQUID readout: $\eta = 0.7$, $N_{\rm sq} = 4$, $S_\Phi^{1/2} = 0.4\,\mu\Phi_0/\sqrt{\rm Hz}$, $T = 4\,$K.

The canonical inputs in one place; beam values from the HSR design of Ref. [1].

Backup: arc and snake spin matrices ◂ lattice

Hexagonal six-snake model: six arcs ($\theta = \pi/3$) and six 180° snakes; spin transport in $SO(3)$.

Arc of orbital bend θ, spin angle $\varphi(\theta) = G\gamma\theta$:

$$\mathrm{R}_{\mathrm{arc}}(\theta) = \mathrm{R}_y(\varphi(\theta)), \quad \mathrm{R}_y(\varphi) = \begin{pmatrix} \cos\varphi & 0 & \sin\varphi \\ 0 & 1 & 0 \\ -\sin\varphi & 0 & \cos\varphi \end{pmatrix}$$

Snake k (180° about $\vec{n}_k = \sin\phi_k\,\vec{e}_x + \cos\phi_k\,\vec{e}_z$):

$$\mathrm{R}_{\mathrm{snake}}(\phi_k) = \begin{pmatrix} -\cos 2\phi_k & 0 & \sin 2\phi_k \\ 0 & -1 & 0 \\ \sin 2\phi_k & 0 & \cos 2\phi_k \end{pmatrix}$$

One-turn map at azimuth s_0:

$$\mathrm{M}(s_0) = \prod_{k=6}^{1} \mathrm{R}_{\mathrm{snake}}(\phi_k)\,\mathrm{R}_{\mathrm{arc}}(\tfrac{\pi}{3})$$

- $\mathrm{M}(s_0) \in SO(3)$, eigenvalues $\{1, e^{\pm 2\pi i\nu_s}\}$; $\lambda{=}1 \Rightarrow$ stable axis $\vec{n}_0(s_0)$, and $\mathrm{tr}\,\mathrm{M} = 1 + 2\cos(2\pi\nu_s)$
- Each arc leaves S_y and each snake flips it; after six snakes $S_y \to +S_y$, so $\vec{n}_0 = \vec{e}_y$ in the arcs (any $G\gamma$)

Six arcs about $\vec{e}_y$ and six 180° snakes compose to a one-turn $SO(3)$ map with $\vec{n}_0 = \vec{e}_y$.

Backup: phasor derivation of $\nu_s = \frac{1}{2}$ ◂ precession

In the xz plane use $w = S_x + iS_z$: a rotation by β is $\times e^{i\beta}$, a reflection is conjugation. Per sector ($\theta = \pi/3$),

$$\begin{aligned} \text{arc:} \quad & w \to e^{-iG\gamma\theta}\, w \\ \text{snake } k: \quad & w \to -e^{-2i\phi_k}\, \bar{w} \end{aligned}$$

Each snake's conjugation flips the preceding arc phase $e^{-iG\gamma\theta} \to e^{+iG\gamma\theta}$, cancelling the next arc; a pair gives $w \to e^{2i(\phi_1 - \phi_2)} w$.

The energy-dependent arc phase drops out; after three pairs the one-turn map is a pure rotation

$$w_{\text{final}} = e^{i\Phi} w_0, \quad \Phi = -2 \sum_{k=1}^{3} \left(\phi_{2k} - \phi_{2k-1}\right)$$

Φ depends only on the snake axes ϕ_k, not on $G\gamma$; matching $e^{\pm 2\pi i \nu_s}$ gives $\nu_s = \frac{1}{2} \iff \Phi = \pi$ at every energy.

ν_s is fixed by the snake axes alone: $\Phi = \pi \Rightarrow \nu_s = \frac{1}{2}$, at all energies.

Backup: Lee-Courant and DLC snake axes ◂ $\vec{n}_0(s)$

The axes $\{\phi_k\}$ leave $\nu_s = \frac{1}{2}$ at every energy but set $\vec{n}_0(s)$ and the amplitude-dependent spin-tune spread (ADST) that limits coherence.

$$\boxed{\begin{aligned} \text{LC:}\quad \phi_k &= (-1)^{k+1}\,45^\circ \\ \text{DLC:}\quad \phi_k &= \psi + (k-1)\,45^\circ \end{aligned}}$$

- LC: successive axes 90° apart [19]; alternating $\pm 45^\circ$ gives $\vec{n}_0 = \vec{e}_y$ in the arcs
- DLC [9]: neighbors step 45°; tracking optimum $\psi \simeq 22.5^\circ$ [20] suppresses resonance driving over the full ramp with static axes

ADST spin-tune-spread scales [20]

Configuration	σ_{ν_s}
DLC	$\lesssim 10^{-2}$
LC	0.02 to 0.04
general axes	0.04 to 0.08
working (baseline)	10^{-3}

Snake axes fix $\nu_s = \frac{1}{2}$ regardless; LC/DLC choice sets $\vec{n}_0$ and spin-tune spread that limits coherence.

Backup: flux per bunch pass ◂ flux signal

– Field and flux per pass

- coil field sets per-turn and SQUID-input flux
- peak γ-enhanced, but $\int B_x^{\mathrm{lab}}\,dz$ is boost-invariant $\Rightarrow \gamma = 1$

$$B_x^{\mathrm{lab}} = +\frac{\mu_0}{4\pi}\,2m_x/r_{\mathrm{coil}}^3$$
$$\Phi_{\mathrm{bunch}} = \frac{\mu_0}{4\pi}\,\frac{|m_x|}{r_{\mathrm{coil}}^3}\,A\,f_{\mathrm{geom}}$$
$$\Phi_{\mathrm{pickup}} = N_{\mathrm{turns}}\,\eta\,\Phi_{\mathrm{bunch}}$$

– $|m_x| = N_p\mu_p$ at $P = 1$, $\sin\alpha = 1$

– pulse $\Delta t \approx 2\sigma_t \approx 0.40\,\mathrm{ns}$: too brief for the time domain; matched filter recovers it

– Coupling factors

- A: single-turn effective coupling area
- $f_{\mathrm{geom}} \sim$ 1-3: longitudinal form factor (saddle-integrated, normalized to on-axis $1/r_{\mathrm{coil}}^3$; sets only the scale)
- N_{turns} windings; η flux-transformer coupling

η, N_{squids}, $S_\Phi^{1/2}$: parameters backup; geometry (r_{coil}, A, f_{geom}, N_{turns}): pickup-geometry backup.

per pass ($\mu\Phi_0$)	inj	flat
Φ_{bunch} (P=1)	17.6	4.41
Φ_{pickup} (P=1)	1236	309

Order $10^3\,\mu\Phi_0$ per bunch at the SQUID input, scaled by $P\sin\alpha$ and recovered coherently.

Backup: the single-pass flux integral ◂ flux signal

- **Instantaneous flux** (one saddle turn)
  - as the bunch passes: $\Phi_1(t) = A\, B_x^{\mathrm{lab}}(t)$
- **The observable is its integral**
  - the matched filter sums the pulse
  - at $\omega_s \sigma_t \sim 10^{-4} \ll 1$ it reads the area
  - change variable $z = vt$:

$$\boxed{\widetilde{\Phi}_1 = \int \Phi_1\, dt = \frac{A}{v} \int B_x^{\mathrm{lab}}\, dz}$$

- **Why it is boost-invariant**
  - transverse field up by γ: $B_x^{\mathrm{lab}} = \gamma B_x'$
  - pulse length down by $1/\gamma$ (Weizsäcker-Williams [21, 22])

$$\boxed{\int B_x^{\mathrm{lab}}\, dz = \int B_x'\, dz' \quad (\gamma^0)}$$

- **Consequences**
  - Pulse peak is γ-enhanced, area not $\Rightarrow \gamma = 1$ in template
  - $\sigma_L \gg r_{\mathrm{coil}}/\gamma$: bunch long against the contracted near field

SQUID records flux integral, not peak: γ amplitude and $1/\gamma$ compression cancel, so $\gamma = 1$.

Backup: matched-filter coherent summation

matched filter

Bunch j, turn n (sign s_j, phase $\psi_j = \pi j / N_{\text{fill}}$):

$$\boxed{x_{j,n} \propto \Phi_{\text{pickup}}\, s_j\, P \sin\alpha\, \cos(\pi n + \psi_j)}$$

πn is the $\nu_s = \frac{1}{2}$ turn flip. Weighting by $w_j = s_j\, e^{-i\psi_j}$ aligns every bunch before summing:

$$\boxed{\left|\sum_j w_j\, x_{j,n}\right| \propto N_{\text{fill}} \quad (\text{uncorrected} : 1)}$$

Coherent integration over T, with $P_\perp = P \sin\alpha$:

$$\boxed{\mathrm{SNR}(T) = K_{\text{template}}\, P_\perp \sqrt{T}}$$

$$\boxed{K_{\text{template}} = \frac{\Phi_{\text{pickup}}}{S_\Phi^{1/2}} \sqrt{N_{\text{fill}}\, f_{\text{rev}}\, \tau_h\, N_{\text{squids}}}}$$

- saddle: $K_{x,y} \approx 1108$ (inj), 277 (flat) $\mathrm{s}^{-1/2}$
- one record: $\mathrm{SNR}_1 \approx 1.2$ at $\sigma_{\nu_s} = 10^{-3}$

Known sign and lattice phase let every bunch add in phase: SNR grows as $\sqrt{N_{\text{fill}}\, f_{\text{rev}}\, T}$.

Backup: coherence time and linewidth

coherence

Reversible dephasing from the spin-tune spread sets the FID envelope $e^{-t/\tau_{\rm coh}}$:

$$\boxed{\begin{aligned} \sigma_f &= f_{\rm rev}\,\sigma_{\nu_s} \quad \text{(FID linewidth)} \\ \tau_{\rm coh} &= \frac{1}{2\pi f_{\rm rev}\sigma_{\nu_s}} = \frac{1}{2\pi\sigma_f} \equiv T_2^* \end{aligned}}$$

with $f_s = \nu_s f_{\rm rev} = 39.07\,\text{kHz}$. A phase-locked π (spin echo) refocuses the reversible part, extending coherent integration beyond $\tau_{\rm coh}$ and separating it from true depolarization.

Config	σ_{ν_s}	σ_f	$\tau_{\rm coh}$
canonical	10^{-3}	78 Hz	2.04 ms
DLC	$\lesssim 10^{-2}$	0.78 kHz	0.20 ms
LC	2×10^{-2}	1.56 kHz	0.10 ms

The canonical $\sigma_{\nu_s}^{\rm eff} = 10^{-3}$ is the working baseline; better-tuned lattices give narrower lines and longer coherence.

The spin-tune spread fixes the FID linewidth and coherence time; the spin echo recovers reversible dephasing, so integration is not capped at $\tau_{\rm coh}$.

Backup: pickup-coil geometry

pickup basis

Transverse saddle (cosine-θ, sine-θ)

Parameter	Symbol	Value
Former radius	r_{coil}	40 mm
Base half-length	L_{base}	7.5 mm
Turn increment	ΔL	1.0 mm
End-loop height	H_{end}	4.5 mm
Max saddle angle	θ_{max}	75°
Windings	N_{turns}	100
Total length	L_z	222 mm
Coupling area	A	40 cm^2
Form factor	f_{geom}	1.5

Axial gradiometer (P_z)

Parameter	Symbol	Value
Loop radius	r_{coil}	40 mm
Baseline	Δz	300 mm

Two NbTi loops in series opposition on the same Macor former, with $L_z = 2[L_{\mathrm{base}} + (N_{\mathrm{turns}} - 1)\Delta L + H_{\mathrm{end}}]$.

One station: a multi-turn cosine-θ and sine-θ saddle pair plus a coaxial axial gradiometer, all on one 40 mm *former.*

Backup: π-pulse field requirements ◂ cycle

All three pulses (tip, π, restore) rotate about $\vec{e}_z$. Tipping $\alpha = 30\,\mathrm{mrad}$ needs $0.84\,\mathrm{T\,m}$ (inj), $9.85\,\mathrm{T\,m}$ (flat); a single-shot π is $105\times$ larger, so spread it over N passes synchronized at f_s:

$$\alpha = \frac{1+G}{B\rho}\int B_z\,dl$$

$$\int B_z\,dl\Big|_{\pi,\text{pass}} = \frac{1}{N}\frac{\pi B\rho}{1+G}, \qquad N \le \frac{1}{4\pi\sigma_{\nu_s}}$$

σ_{ν_s}	τ_{coh}	N	inj ($\int B_z\,dl\|_\pi$, T m)	flat
10^{-2}	0.20 ms	8	11	129
10^{-3}	2.04 ms	80	1.1	12.9
10^{-4}	20.4 ms	796	0.111	1.30

At canonical $\sigma_{\nu_s} = 10^{-3}$ the per-pass field matches the tipping kicker (restore $\simeq 99\%$ of π).

Spreading the π over $\sim$80 synchronized passes brings the per-pass field down to the tipping-kicker level, one kicker for all three pulses.

Backup: finite bunch-length convolution

◂ angular basis

Each channel's point-dipole response is convolved with the Gaussian bunch profile $\lambda(z')$:

$$\lambda(z') = \frac{1}{\sqrt{2\pi}\,\sigma_L}\, e^{-z'^2/2\sigma_L^2}$$

$$g_{T,z}(z_b) = \int \lambda(z')\, h_{T,z}(z_b - z')\, dz'$$

h_T, h_z are the point-bunch transverse (cosine-θ, sine-θ) and axial responses. At injection $\sigma_L \gtrsim r_{\rm coil}$ ($\sim$4 cm) washes out the peak; at flattop the shorter bunch favors the axial channel.

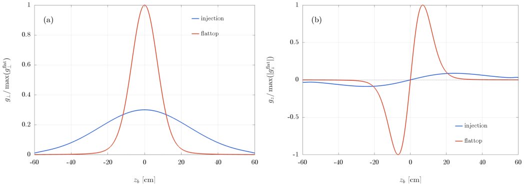

(a) unipolar transverse template g_T; (b) bipolar axial template g_z. Injection and flattop σ_L, normalized to the flattop peak.

Finite bunch length convolves the point response with $\lambda(z')$: at injection $\sigma_L \gtrsim r_{\rm coil}$ washes out the peak, setting the true per-channel amplitudes.

Backup: RF Wien filter at $\nu_s = \frac{1}{2}$ outlook

Operated at the spin resonance $f_{\mathrm{RF}} = (k + \nu_s) f_{\mathrm{rev}}$. A linearly oscillating field carries two counter-rotating components:

$$\boxed{B_x(t) = B_0 \cos\omega t = \frac{B_0}{2}\left(e^{+i\omega t} + e^{-i\omega t}\right)}$$

so resonance has two branches (with $Q_{\mathrm{osc}} = f_{\mathrm{RF}}/f_{\mathrm{rev}}$):

$$\boxed{\nu_s = Q_{\mathrm{osc}} \qquad \nu_s = 1 - Q_{\mathrm{osc}}}$$

Away from $\nu_s = \frac{1}{2}$ the branches separate and one sense is resonant. At $\nu_s = \frac{1}{2}$ they are degenerate: both senses resonate, so a linear field defines no unique rotation axis. A single rotating component is recovered with two orthogonal fields 90° out of phase:

$$\boxed{B_x \propto \cos\omega t, \quad B_z \propto \sin\omega t}$$

RHIC's spin flipper instead used AC dipoles with DC rotators to suppress the unwanted branch [23].

At $\nu_s = \frac{1}{2}$ the two Wien-filter resonance branches coincide; a circularly rotating (90°-phased) field selects one sense for a clean flip.

Backup: Sokolov-Ternov in the ESR

Synchrotron radiation flips spins at unequal rates $W_{\uparrow\downarrow} \neq W_{\downarrow\uparrow}$, building an equilibrium polarization antiparallel to $\vec{B}$ (for e^-) [24]:

$$\frac{1}{\tau_p} = \frac{5\sqrt{3}}{8} \frac{r_e \hbar}{m_e} \frac{\gamma^5}{\rho^3}, \qquad P_\infty = \frac{8}{5\sqrt{3}} \approx 92.4\%$$

The sum $W_{\uparrow\downarrow} + W_{\downarrow\uparrow} = 1/\tau_p$ sets the rate, the difference sets P_∞. Down (against-$\vec{B}$) bunches depolarize faster than up, so the ESR swap-out scheme refreshes them $\sim$every min vs $\sim$3 min for up at 18 GeV, also offsetting *ep* losses [25].

E	γ	B	τ_p
5 GeV	9.8×10^3	0.08 T	$\sim$5 days
10 GeV	2.0×10^4	0.17 T	$\sim$4 h
18 GeV	3.5×10^4	0.30 T	$\sim$12 min

$\rho \approx 200\,\mathrm{m}$ (arcs), $B = p/e\rho$, ideal flat ring, $\tau_p \propto E^{-5}$. Spin rotators add radiative depolarization that shortens the usable time, sharply at 18 GeV.

The ESR self-polarizes to $\sim$92% antiparallel to $\vec{B}$; τ_p runs from days at 5 GeV to minutes at 18 GeV ($\propto E^{-5}$), with opposite outcomes for the two spin states.

Backup: radiative depolarization (Derbenev-Kondratenko)

◂ Sokolov-Ternov ▸ sketch

In a real ring the invariant spin axis $\vec{n}(s;\delta)$ depends on energy, $\vec{n}' \equiv \partial\vec{n}/\partial\delta \neq 0$. Each emitted photon jumps δ stochastically; the spin, aligned with $\vec{n}$, is left misaligned and diffuses, so polarization decays. It dominates where $\vec{n}'$ is large, near spin resonances and in the spin rotators.

$$\boxed{\frac{1}{\tau_{\mathrm{dep}}} = \frac{5\sqrt{3}}{8}\frac{r_e\hbar\gamma^5}{m_e}\frac{1}{C}\oint ds\left\langle \frac{1}{|\rho|^3}\,\frac{11}{18}\,|\vec{n}'|^2\right\rangle}$$

Equilibrium along $\vec{n}_0$ (DKM), with $\vec{n}' = \partial\vec{n}/\partial\delta$:

$$\boxed{P_{\mathrm{dk}} = -\frac{8}{5\sqrt{3}}\frac{\oint ds\,\langle|\rho|^{-3}\,\vec{b}\cdot(\vec{n}-\vec{n}')\rangle}{\oint ds\,\langle|\rho|^{-3}(1-\frac{2}{9}(\vec{n}\cdot\vec{v})^2+\frac{11}{18}|\vec{n}'|^2)\rangle}}$$

Net $1/\tau_p = 1/\tau_{\mathrm{ST}} + 1/\tau_{\mathrm{dep}}$, $P_{\mathrm{eq}} = P_{\mathrm{dk}}$. At 18 GeV the rotators and high γ make $\vec{n}'$ large, so depolarization is fast. [26, 27, 28]

Radiative depolarization adds to ST buildup, $1/\tau_p = 1/\tau_{\mathrm{ST}} + 1/\tau_{\mathrm{dep}}$, so the usable polarization time falls below the bare ST values, well under the $\sim$12 min at 18 GeV where $\vec{n}'$ is large in the rotators.

Backup: the depolarization mechanism

equations

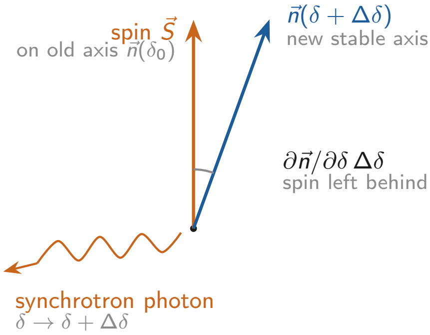

A radiated photon suddenly changes the energy $\delta = \Delta p/p$. Because the stable axis depends on energy, it tilts by $\partial\vec{n}/\partial\delta\,\Delta\delta$; the spin, still on the old axis, is left misaligned and precesses about the new one.

Over many random photons the kicks add up as a spin random walk, so the polarization diffuses away. The strength is set by $|\partial\vec{n}/\partial\delta|^2$: tiny in a matched ring, large near resonances and in the spin rotators.

Each photon tilts the energy-dependent spin axis and leaves the spin behind; many kicks diffuse the polarization, fast where $\partial\vec{n}/\partial\delta$ is large.